

Highly conductive double perovskite oxides A_2LuTaO_6 (A= Ba, Sr, Ca) as promising photoanode material for dye sensitized solar cells

Md Sariful Sheikh^{1,2}, Anurag Roy², Shubhranshu Bhandari², Tapas K Mallick², Senthilarasu Sundaram^{2,*}, T. P. Sinha¹

¹ Department of Physics, Bose Institute, 93/1, A. P. C. Road, Kolkata-700009, India

² Environment and Sustainability Institute, University of Exeter, Penryn Campus, Penryn-TR10 9FE, UK

*Corresponding Author

Email: s.sundaram@exeter.ac.uk

Abstract:

Poor electrical conductivity, interfacial charge carrier recombination, electrode degradation, etc., restrict practical implementation of the TiO_2 based dye sensitised solar cells (DSSCs). In this respect, double perovskite oxides (DPOs) A_2LuTaO_6 (A = Ba, Sr, Ca) have been introduced as the promising DSSC photoanode. These solid-state synthesised DPOs exhibit a suitable wide band gap in the range of 2.94 to 4.07 eV, and 10^4 times higher order of electrical conductivity than TiO_2 . This study reveals that the crystal structure and hence the physical properties of these DPOs can also be easily modulated as required by varying its composition.

Keywords: Double perovskite; Conductivity; Band Gap; Photoanode; DSSC.

Introduction:

Among various available third generation photovoltaic technologies, dye sensitised solar cell (DSSC) technology draws a significant research interest due to its very simple and low-cost fabrication technique [1-3]. As of now, binary TiO_2 (band gap, $E_g \sim 3.2 - 3.4$ eV) based photoanode have shown the best performance for DSSC application [3, 4]. However, poor electron mobility, interfacial carrier recombination, electrode degradation along with the difficulty to control its opto-electronic properties as it has only two components, limit its DSSCs performance [5-6]. In this respect, perovskite materials are viable options for DSSC fabrications, since they have interesting photo physical properties easily tailorable by

doping/alloying. Some ABO₃ type ternary perovskite oxides like, BaSnO₃, SrSnO₃, etc., with higher electrical conductivity, better stability in acidic dye and resistant to photo bleaching, have already shown their potential in DSSC application [6, 7]. Generally, perovskites show high dielectric constant (ϵ') which helps to reduce the charge carrier recombination rate by dielectric screening the various recombination centres i.e. lattice defects and impurities [8]. However, quaternary A₂B'B''O₆ type double perovskite oxides (DPOs) which exhibit better control to the electronic structure compared to its ABO₃ counterpart remain unexplored in DSSC technology. Therefore, exploring the wide band gap DPO photoanode family among the vast array of its related derivatives is of great importance in DSSC science.

In this work, we have introduced DPOs A₂LuTaO₆ (A = Ba, Sr, Ca) as the promising photoanodes for DSSC. Density functional theory (DFT) calculations show that Ba₂LuTaO₆ (BLT), Sr₂LuTaO₆ (SLT) and Ca₂LuTaO₆ (CLT) are wide band gap semiconductors with theoretical band gap of 2.8, 3.47 and 3.91 eV, respectively [9]. BLT and SLT have also shown their potential in photocatalytic waste water treatment and good photo sensitivity under white light illumination [10]. All these reported results suggest that these DPOs may be a promising candidate for DSSC application. Hence, the opto-electronic properties of A₂LuTaO₆ are studied and their effective performance in DSSC is evaluated for the first time.

Results and Discussion:

The crystal structure of the DPOs is studied using X-ray diffraction (XRD) followed by the Rietveld refinement as shown in **Fig. 1(a-c)** and the important lattice parameters are reported in **Table S1**, which are in good agreement with the previous report [9]. In room temperature BLT possesses the cubic structure (Fm3m) with tolerance factor (T_f) 0.99, close to unity. Both SLT and CLT share the distorted monoclinic structure (P2₁/n) with the respective T_f of 0.93 and 0.90. The lattice distortion in this A₂B'B''O₆ structure is inversely proportional to the radius of the A-site cation which is visualised in the schematic unit cell representation of

the DPOs as shown in **Fig. 1(d-f)**. The TEM images as shown in **Fig. 1(g-i)** represent the variety of shapes and sizes in the DPO powders. BLT sample consists of flake-like structure having an average diameter of 38 nm. TEM image of SLT sample shows a mixture of rod (diameter ~ 33 nm) and particle (diameter ~ 10-20 nm) like shapes. Whereas, CLT particles are round shaped in nature with relatively larger diameter of 127 nm. The digital images of the as prepared powders are shown in **Fig. S1**.

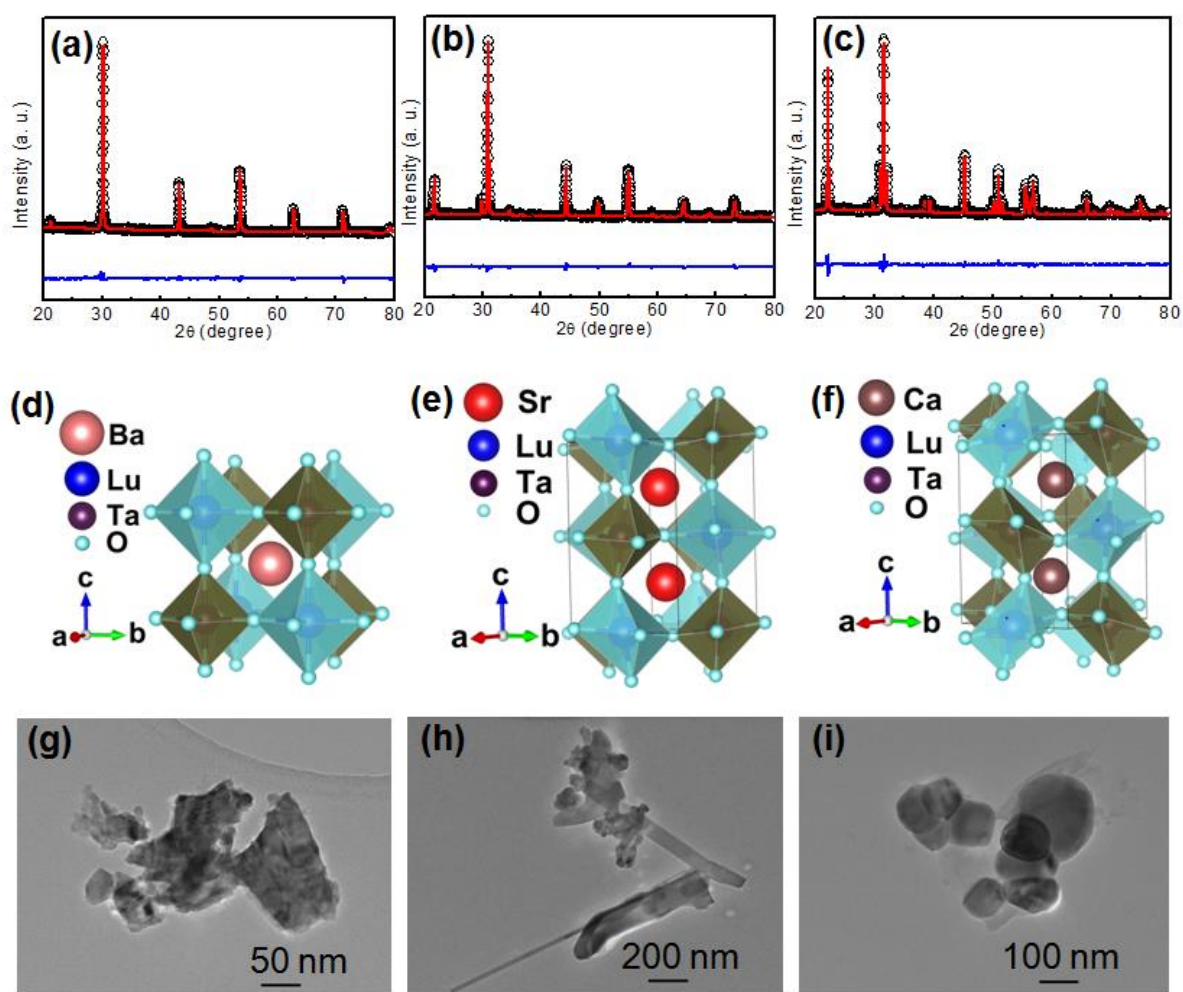


Fig. 1. XRD pattern of (a) BLT, (b) SLT and (c) CLT; symbols, red line and blue line represent the experimental data, simulated data and difference between them, respectively. Unit cell representation of (d) BLT, (e) SLT and (f) CLT; bright field TEM images of (g) BLT, (h) SLT, (i) CLT.

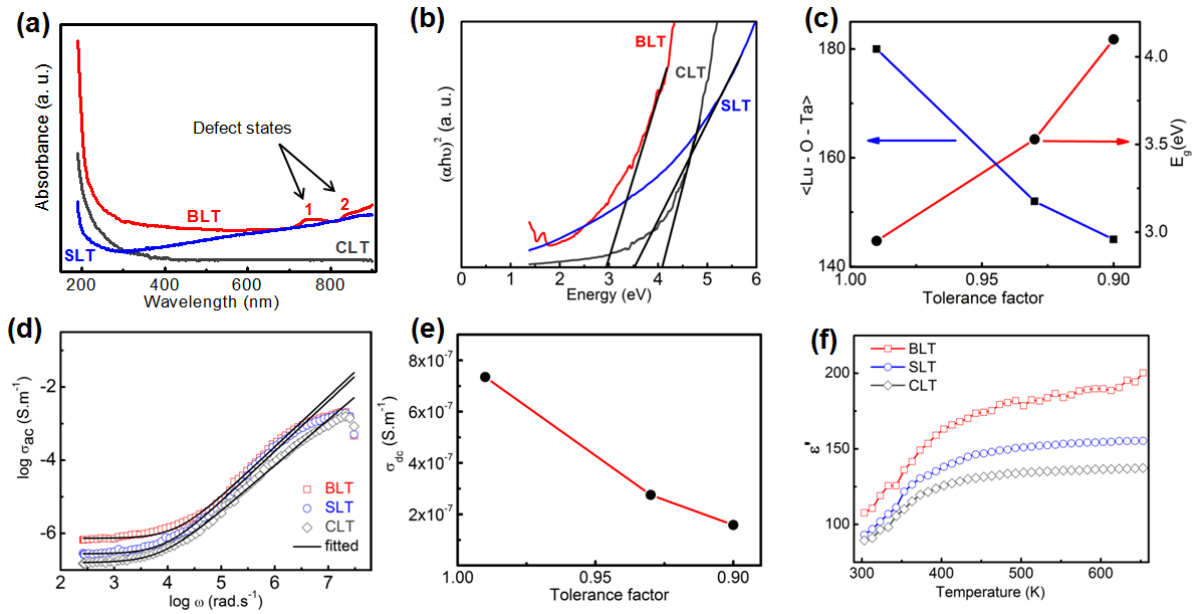


Fig. 2. (a) UV-visible absorption spectra, (b) Tauc plot, (c) T_f dependence of average bond angle and E_g , (d) Ac conductivity plot at 303 K, (e) T_f dependence of σ_{dc} , (f) temperature dependence of ϵ'' .

The UV-visible absorption spectra of the DPOs (Fig. 2a) show the sharp increase in the absorption at the band gap edge which indicates the direct nature of the band gap, consistent with the previous DFT calculations [10]. Two broad and small peaks (1 and 2) within the band gap of BLT as shown in Fig. 2(a) suggest the possibility of the presence of the defect states [11]. However, no similar peaks of defect states are observed in the SLT and CLT absorption spectra. The direct band gaps of BLT, SLT and CLT as obtained from the Tauc plot, shown in **Fig. 2(b)**, are 2.94, 3.53, 4.07 eV, respectively. The electrical properties near the valence band maximum of these materials are determined by the strong hybridisation between (Lu-4f/Ta-5d) and O-2p orbital [9]. From BLT to CLT, the average $\langle \text{Lu} - \text{O} - \text{Ta} \rangle$ bond angle gradually decreases from 180° as shown in **Fig. 2(c)**, which in turn reduces the hybridisation strength of the (Lu-4f/Ta-5d) and O-2p bonds. As the hybridisation strength decreases, the valence band maximum goes down to the lower energy level and the E_g value

gradually increases from BLT to CLT. **Fig. 2(c)** represents the correlation between the lattice distortion and band gap of perovskite structure.

Fig. 2(d) represents the logarithmic angular frequency, $\log\omega$ dependence of the room temperature conductivity. The conductivity in the low frequency plateau region is approximately equal to its dc value (σ_{dc}). As the frequency increases, the conductive states in DPOs become more active to promote the hopping of the charge carriers and conductivity increases nonlinearly as the frequency exceeds the critical hopping frequency (ω_H). The bulk conductivity of the DPOs can be explained using the following Jonscher power law [12]

$$\sigma(\omega) = \sigma_{dc} \left[1 + \left(\frac{\omega}{\omega_H} \right)^n \right] \quad (1)$$

where, n is a dimensionless parameter which varies from 1 to 2. The σ_{dc} value obtained from the Jonscher power law fitting of the conductivity data is plotted in **Fig. 2(e)** which shows that σ_{dc} decreases from BLT to CLT in a similar fashion to T_f . Interestingly, the order of room temperature σ_{dc} ($\sim 10^{-7} \text{ S.m}^{-1}$) in DPOs is quite higher than TiO_2 . Omar et al. (2012) reported that the low frequency room temperature conductivity in TiO_2 single crystal is in the order of $10^{-11} \text{ S.m}^{-1}$ [13].

The temperature dependent real part of the dielectric constant (ϵ') at 1.1 MHz is shown in **Fig. 2(f)**. The room temperature ϵ' value for BLT, SLT and CLT are found to be 107, 93 and 89 respectively, much higher than the ϵ' of TiO_2 (~ 33) [14]. The high values of the ϵ' and σ_{dc} are favourable for the reduced charge carrier recombination rate and efficient electron transport in these DPO photoanodes.

Fig. 3(a) shows the current density - voltage (J - V) characteristics of the fabricated devices and observed photovoltaic parameters are further tabulated in **Table 1**, which indicates that SLT results the highest power conversion efficiency (PCE) of 0.45 % with an open circuit voltage (V_{OC}) of 0.78 V and fill factor (FF) of > 64 %. **Fig. 3(b)** shows the

external quantum efficiency (EQE) plots of the DSSCs and the corresponding values has been given in **Table 1**. The digital images of the fabricated DSSCs are shown in **Fig. S2**. The typical Nyquist plots (**Fig. 3c**) are fitted using an equivalent electrical circuit as shown in the inset of **Fig. 3(c)**. The fitted parameters, R_s , R_{CT} and C denote the series resistance, electron transfer at the DPO/dye/electrolyte interface and chemical capacitance, respectively, are shown in **Table 1**. Higher value of R_{CT} indicates the more delayed charge carrier recombination at the DPO/electrolyte interface [15]. The highest efficiency of the SLT based DSSCs may be attributed to the absence of any defect states, lowest value of R_s and highest value of R_{CT} . **Fig. 3(d)** shows a schematic of the SLT based DSSC. Due to the relatively larger particle size and low dc-conductivity, R_s almost doubles and R_{CT} decreases significantly in CLT based DSSC which is reflected in its decreased efficiency. **Table S2** shows that these DPOs show good performance as compared to that reported for some other promising oxide photoanode based DSSCs. The promising DSSC performance of these DPOs may be attributed to the higher electrical conductivity and dielectric constant of the perovskite structure.

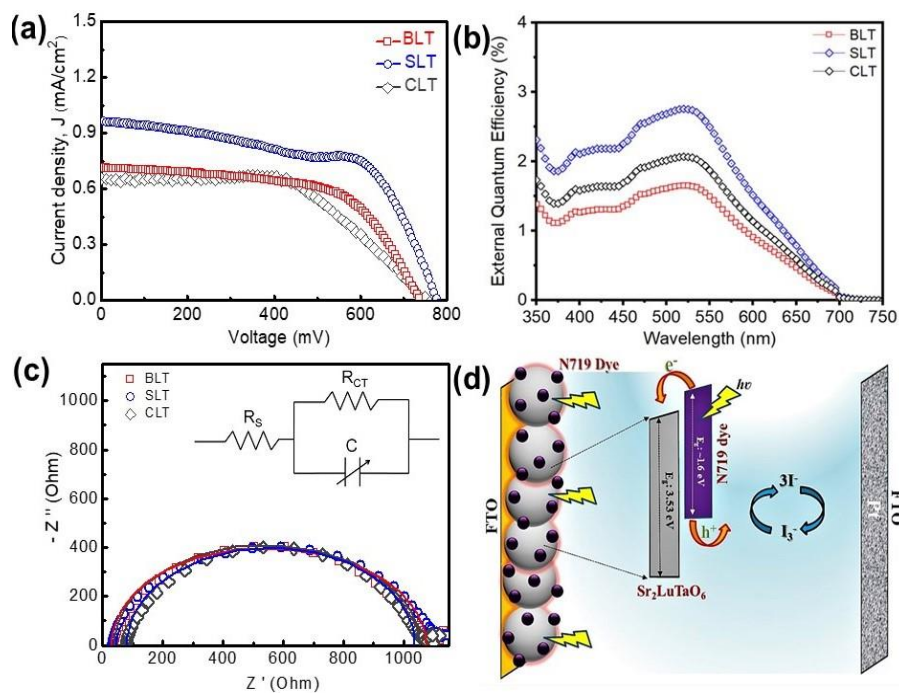


Fig. 3. (a) J-V characteristics of the DSSCs. (b) EQE plots, (c) Nyquist plots of the DSSCs. Inset shows the equivalent electrical circuit, (d) schematic diagram of SLT-based DSSC.

Table 1: Photovoltaic and impedance spectroscopic measurement parameters of the DPO based DSSCs.(Active device area: 0.25 cm ²)								
DPO	V _{OC} (V)	J _{SC} (mA.cm ⁻²)	FF (%)	PCE (%) ± 0.05	R _s (Ω.cm ⁻²)	R _{CT} (Ω.cm ⁻²)	C (10 ⁻⁶ F)	EQE (%)
BLT	0.74	0.71	60.2	0.32	39.2	1035	2.17	2.08
SLT	0.78	0.96	64.3	0.45	30.3	1045	2.06	2.75
CLT	0.76	0.63	61.9	0.28	76.6	975	2.36	1.63

The efficiency of these DPO based DSSCs may be improved by increasing the J_{SC}, V_{OC} and FF. Improvement in J_{SC} is possible by reducing the size and changing the morphologies of the DPO particles for higher surface area which will enhance the dye loading and hence the J_{SC}. The microstructure of DPOs may be varied by using advanced sample preparation techniques like, sol-gel, hydrothermal, facile molten route synthesis, etc. V_{OC} and FF may be improved by optimising the electronic structure of the DPOs, film deposition techniques and device architecture. The electronic structure as well as physical properties can be modulated by optimizing the chemical composition within the DPOs.

Conclusion:

The photovoltaic performance of A₂LuTaO₆ (A = Ba, Sr, Ca) photoanode in DSSC have been studied and a correlation among the crystal structure, materials property and device performance is explored. In future, the synthesis and variation of composition in A₂LuTaO₆ will be of great importance to obtain the optimal photovoltaic performance from these DPOs. These DPOs may also find promising applications as the photoanode in photoelectrochemical water splitting cell, electron transport layer for the halide perovskite solar cell, etc.

Supporting information file: The details of materials synthesis, DSSC fabrication and characterisations are reported in supporting information file.

Acknowledgements:

M.S.S gratefully acknowledges INSPIRE Fellowship program of Department of Science and Technology (DST), Government of India and Newton-Bhabha PhD Fellowship Program (2019-2020) funded by DST, Government of India and British Council.

References:

- [1] B. O'Regan, M. Grätzel, *Nature* 353 (1991) 737-40.
- [2] W.C. Oh et al., *Sci. Rep.* 10 (2020) 4738-10.
- [3] S.S. Shin et al., *Energy Environ. Sci.* 12 (2019) 958-964.
- [4] K. Kakiage et al., *Chem. Commun.* 51 (2015) 15894-15897.
- [5] Y. Zhang et al., *J. Phys. Chem. C* 112 (2008) 8553-8557.
- [6] A. Roy et al., *ACS Sustainable Chem. Eng.* 6 (2018) 3299-3310.
- [7] A.A. Kumar, A. Kumar, J.K. Quamara, *Solid State Commun.* 269 (2018) 6-10.
- [8] M.S. Sheikh et al., *Mater. Chem. Phys.* 244 (2020) 122685-9.
- [9] S. Halder et al., *Ceram. Int.* 43 (2017) 11097-11108.
- [10] S. Halder et al., *Ceram. Int.* 45 (2019) 15496-15504.
- [11] T. Omata, et al., *J. Am. Chem. Soc.* 136 (2014) 3378-3381.
- [12] A.K. Jonscher, *Dielectric Relaxation in Solids*, Chelsea Dielectrics Press, London, 1983.
- [13] M.B. Omar, A. Matoussi, "Dielectric and conductivity investigations of rutile titanium dioxide single crystals," 2012 Annual Report Conference on Electrical Insulation and Dielectric Phenomena, Montreal, QC, 2012, pp. 467-470.
- [14] T. Busani, R.A.B Devine, *Semicond. Sci. Technol.* 20 (2005) 870-875.
- [15] H. Tian et al., *J. Phys. Chem. C* 114 (2010) 1627-1632.